frontiers in Physics

ORIGINAL RESEARCH
published: 02 March 2022
doi: 10.3389/fphy.2022.785627

Time Resolution Studies of Thallium Based Cherenkov Semiconductors

Giulia Terragni[1,2], Marco Pizzichemi[1,2], Emilie Roncali[3,4], Simon R. Cherry[3,4], Jaroslaw Glodo[5], Kanai Shah[5], Gerard Ariño-Estrada[3], Etiennette Auffray[1], Alessio Ghezzi[2] and Nicolaus Kratochwil[1,6]*

[1]European Organization for Nuclear Research (CERN), Meyrin, Switzerland, [2]Department of Physics, University of Milano-Bicocca, Milan, Italy, [3]Department of Biomedical Engineering, University of California, Davis, Davis, CA, United States, [4]Department of Radiology, University of California, Davis, Davis, CA, United States, [5]Radiation Monitoring Devices, Inc., Watertown, MA, United States, [6]Faculty of Physics, University of Vienna, Vienna, Austria

In the context of improving the detector performance of time-of-flight positron emission tomography (TOF-PET), the combination of charge induction readout and prompt Cherenkov photon production in semiconductor materials can lead to an outstanding detector performance in energy, timing, and spatial resolution. Energy resolutions as good as 1.2% at 662 keV and 5% at 122 keV are reported for pixel thallium bromide (TlBr) detectors. The high refractive index of Tl-based materials, between 2.3 and 2.6, leads to a high Cherenkov photon generation yield but can also challenge photon extraction, potentially affecting the time performance. In this work, the timing properties of TlBr and thallium chloride (TlCl) crystals of different geometries are measured using an optimized test setup with high-frequency readout electronics. A coincidence time resolution (CTR) value of 167 ± 6 ps FWHM is achieved using a $3 \times 3 \times 3\,mm^3$ black-painted TlBr crystal. In order to assess potential improvements, a Geant4-based simulation tool kit is developed and validated against experimental measurements. The simulation tool kit is used to predict the contributions limiting the time resolution regarding the crystal and photodetector properties, highlighting the potential of such materials. Finally, paths to further improve the detector performance in TOF-PET are discussed.

Keywords: Cherenkov emission, TlBr crystal, TlCl crystal, silicon photomultiplier (SiPM), TOF-PET, coincidence time resolution (CTR), GEANT4 simulation

OPEN ACCESS

Edited by:
Giovanni Calderini, UMR7585 Laboratoire Physique nucléaire et Hautes Energies (LPNHE), France

Reviewed by:
Ge Yang, North Carolina State University, United States
Han Gyu Kang, National Institutes for Quantum and Radiological Science and Technology, Japan
Luigi Cosentino, Laboratori Nazionali del Sud (INFN), Italy

****Correspondence:***
Giulia Terragni
giulia.terragni@cern.ch

Specialty section:
This article was submitted to Radiation Detectors and Imaging, a section of the journal Frontiers in Physics

Received: *29 September 2021*
Accepted: *25 January 2022*
Published: *02 March 2022*

Citation:
Terragni G, Pizzichemi M, Roncali E, Cherry SR, Glodo J, Shah K, Ariño-Estrada G, Auffray E, Ghezzi A and Kratochwil N (2022) Time Resolution Studies of Thallium Based Cherenkov Semiconductors. Front. Phys. 10:785627. doi: 10.3389/fphy.2022.785627

1 INTRODUCTION

Image quality in positron emission tomography (PET) is primarily determined by the detector performance, and it can be largely improved by better localizing the positron–electron annihilation point. To this aim, the detectors must fulfill several requirements. Spatial resolution and detection efficiency are important since they contribute to determining the overall system resolution. Two other crucial parameters are the coincidence time resolution (CTR) between detector pairs and the energy resolution of the detectors, in order to identify possible scatterings of the detected gamma and discard or correct for it [1]. Inorganic scintillators such as cerium-doped lutetium yttrium orthosilicate (L(Y)SO:Ce), barium fluoride (BaF_2), or bismuth germanate (BGO) coupled to silicon photomultipliers (SiPMs) can achieve CTR values below 100 ps [2–4]; however, their energy resolution is limited to approximately 10% for LYSO [5] and 18% for BGO [6].

High-Z semiconductor gamma-ray detectors, on the other hand, offer significantly better energy resolution. Values between 1 and 2% at 662 keV and 5% at 122 keV are reported for pixelated TlBr

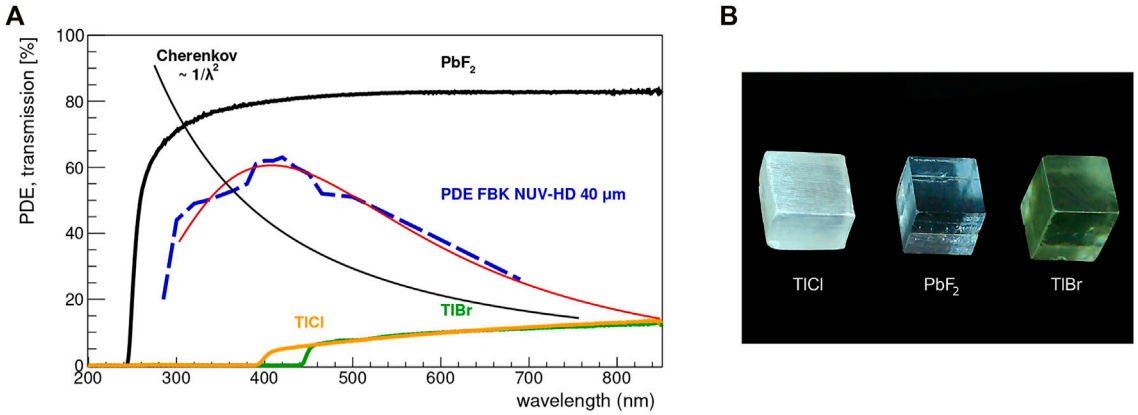

FIGURE 1 | (A) Transmission of 3 × 3 × 3 mm^3 PbF_2, TlBr, and TlCl crystals. The surface conditions of TlBr and TlCl crystals (unpolished) are not optimized as the aim of this measurement is to show the cutoff wavelengths. Greater transmission is expected for polished TlBr and TlCl crystals. In the simulations, transmission is set to 100% independently from the material, since the roughness of the surfaces is separately introduced as well as Fresnel reflections. The PDE of the SiPM is taken from [2] and estimated between the measured points using a polynomial fit function. **(B)** 3 × 3 × 3 mm^3 TlCl, PbF_2, and TlBr crystals observed using the microscope, showing the difference between the polished PbF_2 surface and the unpolished semiconductor crystal surface.

detectors with pixel sizes between 1 and 2 mm and a pixel-to-thickness ratio below 0.2, under different bias voltage and temperature conditions [7, 8]. Provided the relative transparency of TlBr in the visible range, Cherenkov photons are produced upon gamma interaction in the crystal [9] and serve as a very precise time tagger [10]. The combination of charge readout with the detection of the prompt photons [11, 12] can lead to an outstanding detector performance in energy, timing, and spatial resolution with very good detection efficiency. A detailed description of the advantages and disadvantages of this detector design with respect to scintillator-based PET detectors can be found in [12, 13].

CTR values as low as 30 ps FWHM have been reported using microchannel plate photomultipliers (MCP-PMTs) with embedded pure Cherenkov radiators of 5 mm thickness [14]. When using SiPMs and crystals with PET-sized geometry instead, the timing performance deteriorates significantly [15, 16]. Without optimized readout conditions, time resolution values between 300 and 400 ps FWHM have been measured in a proof-of-concept study conducted with TlBr and TlCl crystals [13].

In this contribution, we evaluate the time resolution of TlBr and TlCl semiconductor materials coupled to analog SiPMs from Fondazione Bruno Kessler (FBK) [17] in an optimized test bench [18]. A time-walk correction is introduced to mitigate the impact of cross talk and fluctuations on the signal slew rate. Depth-of-interaction (DOI)-collimated measurements are performed to investigate the impact of light propagation in high refractive index materials, and, in parallel, a Geant4-based simulation tool kit is developed to reproduce the experimental results and to disentangle the relevant contributions limiting the time resolution, regarding the crystal properties (refractive index, cutoff wavelength, surface state, and geometry) and the photodetector parameters [single photon time resolution (SPTR) and photon detection efficiency (PDE)]. Finally, we discuss strategies for further improvements.

2 MATERIALS AND METHODS

2.1 TlBr and TlCl Crystals

TlBr, TlCl, and lead fluoride (PbF_2) crystals with dimensions 3 × 3 × 3 mm^3 are used for this study. The 3 × 3 × 3 mm^3 geometry is of interest to evaluate the intrinsic performance of the crystal as a best-case scenario with low photon time spread and good light transfer efficiency. A 3 × 3 × 20 mm^3 TlBr crystal is also used as it represents the conventional geometry used in PET. One of the 3 × 3 mm^2 faces is coupled to a SiPM using Cargille Meltmount with n = 1.58 and cutoff at 300 nm. The remaining surfaces are Teflon-wrapped or black-painted using a spray with a refractive index n = 1.5 [16], to emphasize the crystal properties. The transmission of the crystals is measured without wrapping, using a PerkinElmer LAMBDA spectrophotometer. **Figure 1** displays the measured transmission as a function of the wavelength on the left. The cutoff for TlCl and TlBr is, respectively, at 400 and 440 nm, extrapolated from the curve at 50% of the slope. The relatively low transmission of TlBr and TlCl, with respect to PbF_2, is the result of the unpolished surface of these crystals. These and other relevant crystal properties are summarized in **Table 1**.

2.2 Coincidence Time Resolution Setup

The measurements of the CTR are performed using the coincidence setup described in [2], where a ^{22}Na source with activity 2.7 MBq is placed between a small reference detector (2 × 2 × 3 mm^3 LSO:Ce:Ca) and the crystal under test, both coupled to 4 × 4 mm^2 FBK NUV-HD SiPMs. The SiPMs are biased at 39 V, about 10 V above breakdown voltage. This setting ensures optimal conditions in terms of timing performance [2]. As described in **Figure 2**, high-frequency electronics is used to monitor the voltage drop between the SiPM anode and cathode with a very fast SiPM single-cell signal rise time, which also measures the number of triggered cells in the SiPM. The electronics of the high-frequency amplifier is

TABLE 1 | Physical properties of the Cherenkov radiators under study and scintillating crystals for comparison.

Material	PbF_2	TlCl	TlBr	$Bi_4Ge_3O_{12}$	LYSO:Ce	BaF_2
Density [g/cm^3]	7.8[a]	7.0[b]	7.5[b]	7.1[a]	7.2[a]	4.9[a]
Z_{eff}[c]	77	76	73	71	64	51
Refractive index at 500 nm[d]	1.78	2.32	2.48	2.14	1.82[a]	1.48
Measured cutoff wavelength [nm]	250	400	440	300	370	<190
Attenuation length [mm] for 500 keV γ[e]	8.7	9.7	9.7	10.1	11.4	22.5

[a] *Epic Crystal datasheet: https://www.epic-crystal.com/*
[b] *From [13].*
[c] *Approximation calculated according to [19].*
[d] *Refractive index database: https://refractiveindex.info/*
[e] *NIST database: https://physics.nist.gov/PhysRefData/Xcom/html/xcom1.html*

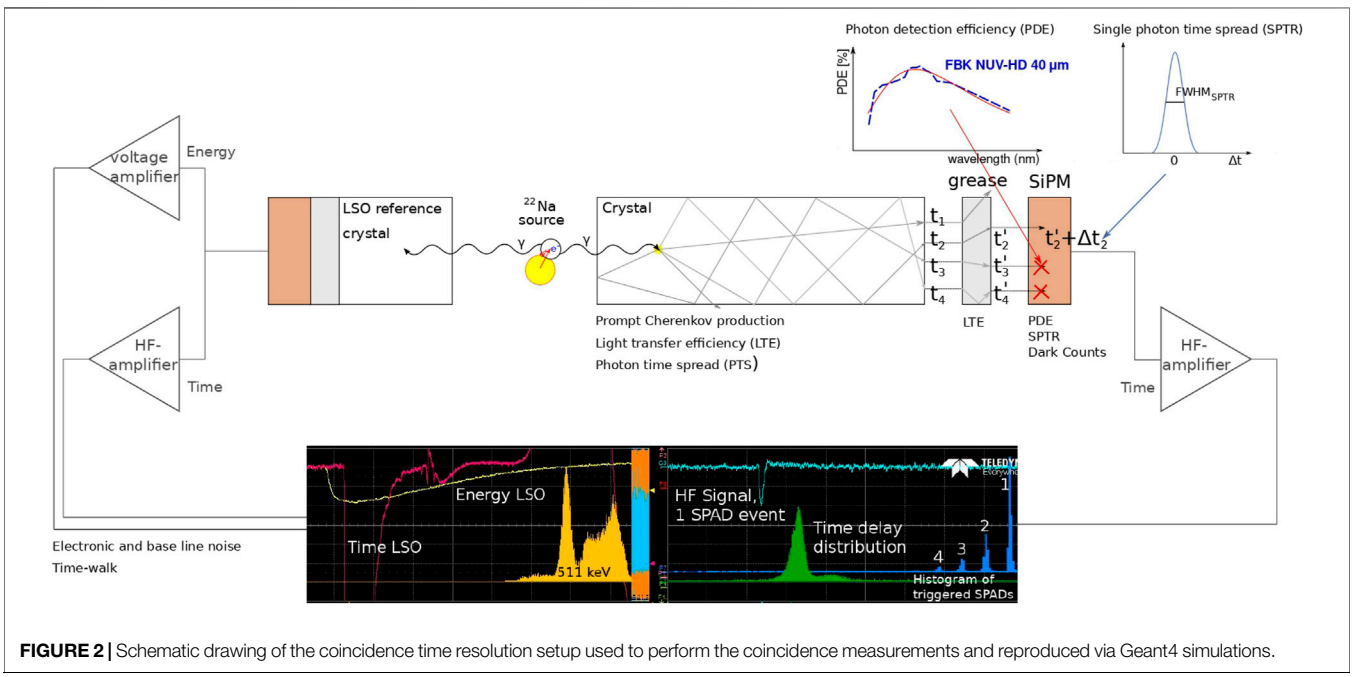

FIGURE 2 | Schematic drawing of the coincidence time resolution setup used to perform the coincidence measurements and reproduced via Geant4 simulations.

described in depth in [18, 20]. The energy deposition in the reference detector is analyzed by integrating the output signal from a unity-gain amplification stage (voltage amplifier). This allows to select 511 keV photoelectric events and to minimize the presence of spurious coincidences in the dataset, due to the events that undergo a scattering process in the vicinity of the crystal. The signals are digitized using a LeCroy DDA735Zi oscilloscope, characterized by 3.5 GHz bandwidth, 20 Gs/s sampling rate (i.e. 50 ps binning), and a leading edge threshold that calculates the signal crossing time via sin(x)/x interpolation. The threshold for the reference detector is set at 20 mV (about 50% of the single-cell signal amplitude), while for the Cherenkov radiator at 10 mV, optimized to reach the best possible time resolution. Since the time information is extracted with a leading edge threshold, signals present a strong time-walk, which is observed in particular for low light intensities [21] or Cherenkov photons [4]. Therefore, a correction method is implemented using the SiPM signal slew rate.

The CTR of the described setup is defined as the full width at half maximum (FWHM) of the distribution of the time-stamps, and it represents the time resolution of the coincidence between the Cherenkov radiator-based detector and the reference detector. To reproduce the CTR assuming two identical detectors in coincidence, the value is multiplied by $\sqrt{2}$, and the resolution of the reference crystal ($CTR_{reference}$ = 61 ± 3 ps from [16]) is subtracted as:

$$CTR = \sqrt{2 \cdot CTR^2_{measured} - CTR^2_{reference}}. \quad (1)$$

When selecting events with one-triggered avalanche diode (SPAD) or one Cherenkov photon detected, the single photon coincidence time resolution (SPCTR) is extracted as FWHM. SPCTR is useful to validate simulations, where SiPM cross talk is not included, and to better understand the fundamentals of light transport.

2.3 Monte Carlo Simulations

A Monte Carlo code based on the Geant4 tool kit is developed to model the experimental apparatus and reconstruct the time

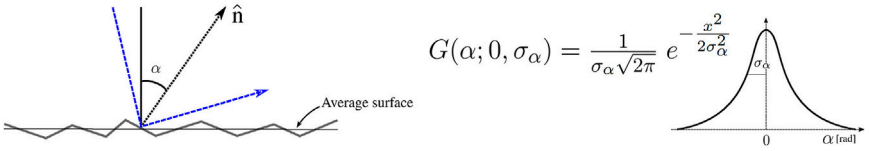

FIGURE 3 | Simulation of the reflection of an optical photon on a surface of the crystal. The σ_α parameter allows the specification of the surface roughness. The unified model assumes that the probability of micro-facet normals populating the annulus of the solid angle sin(α) dα is proportional to a Gaussian with standard deviation σ_α. The constraint on sin(α) is defined as the lower between 1 [sin(π/2)] and 4 σ_α.

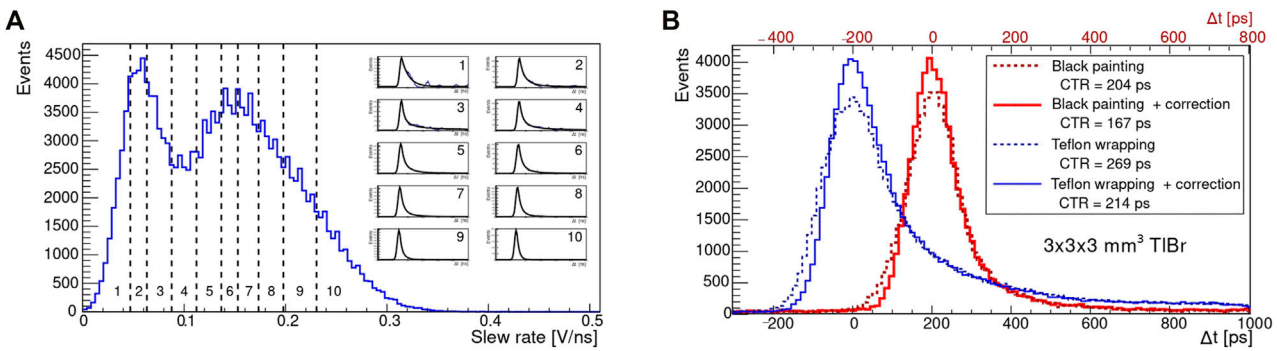

FIGURE 4 | (A) Correction method applied to the case of the Teflon-wrapped 3 × 3 × 3 mm^3 TlBr crystal. The slew rate distribution is divided into 10 categories containing an equal number of events. For each category, the time delay distribution is interpolated to extract the position of the maximum, which is used to perform the correction. **(B)** Measured (dashed) and corrected (solid) time delay distributions for the black-painted and Teflon-wrapped 3 × 3 × 3 mm^3 TlBr crystal and extracted CTR values before and after time-walk correction. The curves referring to the black-painted and Teflon-wrapped crystal are artificially offset by 200 ps for display purposes.

distributions. The geometry and composition of the crystal, optical coupling agent, and silicon photodetector are implemented. A particular focus is put on the model of the crystal surfaces, defined as optical surfaces using the unified model and setting a ground finish. Specular reflections are considered on a surface whose roughness is defined by the σ_α parameter [22, 23]. σ_α describes the Gaussian dispersion of the angle α [rad] between a micro-facet on which an optical photon interacts and the average surface (**Figure 3**).

The electron and Cherenkov light production and transport are tracked and saved for further analysis, together with the energy deposition. The simulation output is processed using the ROOT libraries to include the SiPM properties, hence a jitter in the arrival time due to SPTR and electronic noise, reproduced as Gaussian smearing with σ = 42 ps [2], and a weight to consider the photon detection efficiency as shown in **Figure 1**. The final time distribution is then convoluted with a Gaussian distribution to model the behavior of the reference detector and, finally, an uncorrelated dark count floor is added.

The σ_α parameters are tuned against experimental measurements, and the model is then used to analyze the contributions limiting the time resolution. Moreover, the setup performances are predicted when separately improving the crystal and SiPM properties. Given the complex structure of the time distribution, when studying the impact of the SiPM choice on the CTR, the figure of merit for the time resolution is extracted as the standard deviation within a fixed time window, instead of the FWHM. SiPM cross talk and after pulse effects are not considered in this model.

3 RESULTS

3.1 Coincidence Time Resolution

The 3 × 3 × 3 mm^3 TlBr crystal is measured with the setup described in **section 2.2**. The time delay distribution of the crystal wrapped in Teflon and black-painted is displayed on the right of **Figure 4** with the dashed line. The asymmetry in the distribution originates from the difference in performance between the reference crystal and TlBr. The distribution for the black painted crystal shows a more moderate tail. Indeed, the tail is attenuated when photons that undergo several reflections in the crystal are not detected. Similar behavior is presented in [13] when events with lower amplitude are removed from the dataset. To model the shape, a Crystal Ball fit function is used, which consists of a Gaussian convoluted with an exponential function [16]. The CTR values obtained after correction for the contribution of the reference detector according to **Eq. (1)** are $CTR_{Black\ painting}$ = 204 ± 7 ps and CTR_{Teflon} = 269 ± 9 ps, assuming two identical TlBr crystals in coincidence. Despite the significant improvement in the time resolution achieved by painting the 3 × 3 × 3 mm^3 TlBr black to suppress reflections in the crystal, the overall signal-to-noise ratio is not superior with respect to other reflectors for the low number of coincidence events detected. Aiming to obtain the best detector

TABLE 2 | Summary of the CTR measurements performed using three materials with different refractive indexes and different geometries. The crystal dimensions and wrapping are listed together with the extracted coincidence time resolution (CTR) before and after time-walk correction.

Material	Refractive index	Geometry [mm^3]	Wrapping condition	Surface state	CTR before correction [ps]	CTR after correction [ps]
PbF_2	1.78	3 × 3 × 3	Teflon	Polished	206 ± 7	142 ± 6
TlCl	2.32	3 × 3 × 3	Teflon	Not polished	267 ± 9	210 ± 7
TlBr	2.48	3 × 3 × 3	Black painting	Not polished	204 ± 7	167 ± 6
TlBr	2.48	3 × 3 × 3	Teflon	Not polished	269 ± 9	214 ± 7
TlBr	2.48	3 × 3 × 20	Teflon	Not polished	330 ± 10	285 ± 9

performance, a trade-off between sensitivity and timing must be considered [24]. The measurement is repeated with Teflon-wrapped TlCl and PbF_2 crystals of the same dimensions. The results are summarized in **Table 2** and show agreement between the CTR values of TlCl and TlBr and an improvement using PbF_2.

3.2 Correction Method

The stated CTR values are affected by time-walk due to the leading edge discriminator of the oscilloscope and the low number of triggered SPADs in the SiPM. One strategy to mitigate this effect is to lower the leading edge threshold to just above the electronic noise floor. However, at such low thresholds, the electronic noise would deteriorate the time resolution more than the time-walk itself. Instead, the slew rate at 30 mV (about 75% of the single-cell amplitude) is measured for each event, and a correction method is implemented using this information.

The collected data are divided into 10 categories as shown on the left of **Figure 4**, each one containing the same number of events. For each category, the time delay distribution is separately analyzed, and the position of the maximum is evaluated by interpolation. The coincidence time resolution of the individual categories ranges from 324 to 180 ps, while a shift of the centroid of 110 ps can be observed between the first and last category. The time delay distributions are merged after subtracting for the position of the centroid, thus reducing the smearing due to time-walk. Further details on a similar correction are presented in [4, 25]. After time-walk correction, the values significantly improve. $CTR_{Black\ painting}$ goes from 204 to 167 ps FWHM and CTR_{Teflon} from 269 to 214 ps FWHM (**Figure 4** right).

3.3 Increased Crystal Length

The last measurement listed in **Table 2** is performed with the Teflon wrapped 3 × 3 × 20 mm^3 TlBr crystal. Locating the 3 × 3 mm^2 face in coincidence, the CTR value extracted after time-walk correction is 285 ± 9 ps FWHM. The value is significantly higher than the time resolution of the 3 mm long crystal, arguably due to the time spread introduced by the DOI of the incident gamma photons [26] and a lower LTE with respect to the shorter one [27, 28].

3.4 Depth-of-Interaction-Collimated Measurements and Simulations

To determine the light propagation time in TlBr, the 3 × 3 × 20 mm^3 crystal wrapped in Teflon is used to perform DOI-lateral-collimated measurements along the 20 mm long side of the crystal. The 3 × 20 mm^2 face is located in coincidence, and the reference detector is placed far from the source to have a collimated parallel beam of gamma photons. The source and the reference detector are moved in steps of 1 mm along the 20 mm side, to reproduce different depths of interaction from 0 mm DOI, at the far end of the TlBr crystal, to 20 mm DOI, near the SiPM. The resulting coincidence time delay histograms are displayed in **Figure 5** on the left, selecting events in which only one photon is detected. There is an increasing delay (t_{delay}) in the position of the maximum of the distributions, from 0 to 19 mm of DOI, due to the increasing distance that the produced optical photon must travel in the crystal before being detected, defined as:

$$t_{\mathrm{delay}} = \frac{\bar{x}}{\frac{c}{n}} \quad \text{and} \quad \bar{x} = (20\,\mathrm{mm} - \mathrm{DOI[mm]}) \cdot k, \qquad (2)$$

where $\frac{c}{n}$ is the speed of the optical photons in the crystal and $\bar{x}$ is the average traveled distance. $\bar{x}$ depends on the DOI position, the position of the source, and on a coefficient $k \geq 1$, which takes into account the multiple reflections of the photons on the long lateral sides (3 × 20 mm^2) of the crystal.

A second peak, resolved for DOI positions between 11 and 19 mm, characterizes the time distributions [29, 30]. This peak is created by the photons that are produced toward the far end of the crystal, are back-reflected on the 3 × 3 mm^2 face not coupled to the SiPM, and finally detected. The resolution of the second peak is worse than that of the first one since it contains the time-stamp of photons traveling longer and thus more exposed to fluctuations in the number of internal reflections or lost photons. The time difference between the two peaks is defined as:

$$t_{\mathrm{2nd\,peak}} - t_{\mathrm{1st\,peak}} = \frac{2\,\overline{x'}}{\frac{c}{n}} \quad \text{and} \quad \overline{x'} = (\mathrm{DOI[mm]}) \cdot k. \qquad (3)$$

Geant4 simulations are developed to extract complementary information to the measurements. In particular, the DOI-collimated measurements are used to tune the crystal surface parameters of TlBr in the Geant4 model. To simplify simulations, the correlated noise of the SiPM (cross talk, after pulsing) is not included and, to provide identical conditions between measurements and simulations, only events with one-triggered SPAD (one detected Cherenkov photon) are considered. The tuning of the parameters is required to correctly reproduce the coincidence time spectra since the surface state has a strong impact on the time resolution [31–33]. The lateral surfaces have a different roughness with respect to the front and back; therefore, two different parameters are considered: $\sigma_{\alpha\ 1}$ for the lateral faces and $\sigma_{\alpha\ 2}$ for the back and front. The two

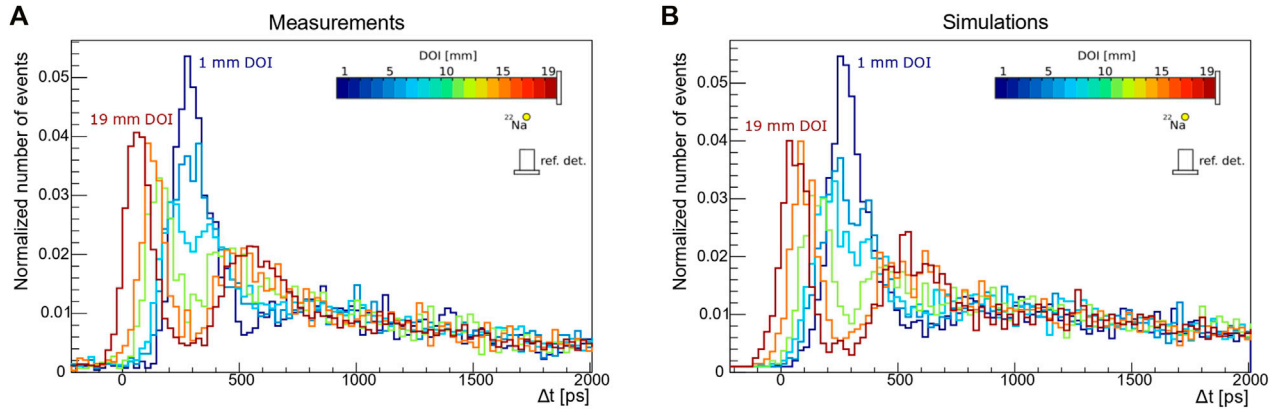

FIGURE 5 | (A) Normalized time delay distributions for lateral DOI-collimated measurements. The measurements are performed by placing the 3 × 20 mm^2 face of the 20 mm long Teflon-wrapped TlBr crystal in coincidence with the reference detector. The source and the reference detector are moved in steps of 1 mm along the 20 mm side. **(B)** Corresponding DOI-collimated simulations.

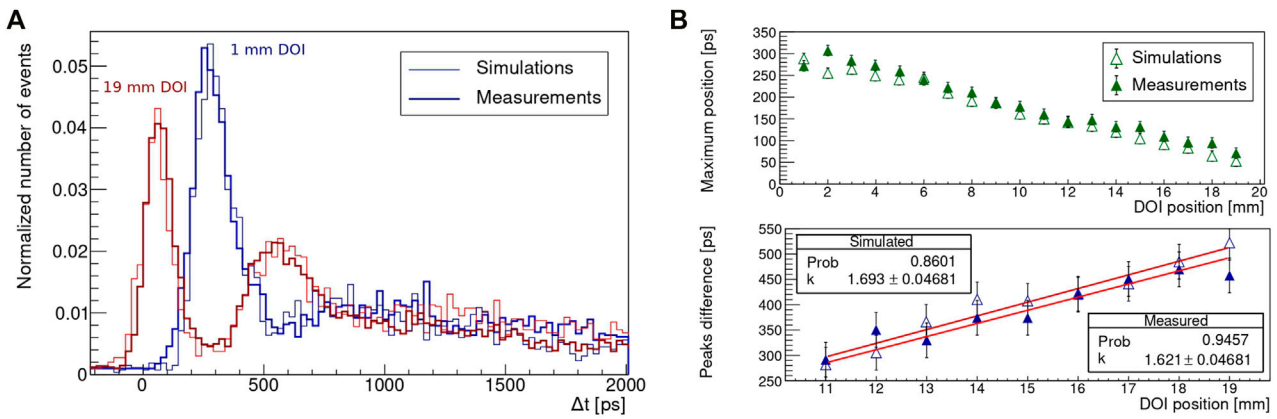

FIGURE 6 | (A) Comparison between the measured and simulated normalized time distributions at the extremes of the crystal, DOI = 1 mm (blue) and 19 mm (red). **(B)** Position of the maximum and distance between the two peaks of the measured and simulated time distributions as a function of DOI. **Eq. (4)** is used to extract the coefficient *k*.

peaks characterizing the measured time distributions are used for the tuning since $\sigma_{\alpha\ 1}$ affects the resolution of both peaks while $\sigma_{\alpha\ 2}$ affects only the second one. Simulations are performed varying the values of $\sigma_{\alpha\ 1}$ and $\sigma_{\alpha\ 2}$. The values that best fit the measurements are $\sigma_{\alpha\ 1} = 0.04 \pm 0.01$ and $\sigma_{\alpha\ 2} = 0.5 \pm 0.1$, compared to typical values of about 0.005–0.01 for a common well-polished surface. The resulting simulations are shown on the right of **Figure 5**, for different DOI positions. The left of **Figure 6** shows the simulated normalized distributions in comparison with the measured ones at the extremes of the crystal, DOI = 1 and 19 mm. The agreement is maintained at all the DOI values: the position of the maximum of the time distribution (t_{delay}), and the difference between the two peaks ($t_{2nd\ peak} - t_{1st\ peak}$) is analyzed as a function of the DOI (**Figure 6** right). From the latter, the *k* coefficient is extracted using **Eq. (3)**, which can be rewritten as:

$$t_{2nd\,peak} - t_{1st\,peak} = \frac{2\,\overline{x'}}{\frac{c}{n}} = \frac{2\,k}{\frac{c}{n}}\,\mathrm{DOI\,[mm]}. \qquad (4)$$

The coefficients extracted from simulations and measurements are:

$$k_{sim} = 1.62 \pm 0.05 \quad \text{and} \quad k_{meas} = 1.69 \pm 0.05. \qquad (5)$$

Moreover, by integration of the baseline of the measured time distributions, the number of dark counts is extracted. Dark counts represent ~15% of the total number of events when events with a single-triggered SPAD are selected. The dark count composition highly depends on the experimental condition and can be lowered by using a stronger radioactive source, a larger reference detector, or decreasing the distance between the two crystals.

3.5 Contributions to the Coincidence Time Resolution

The validated simulation model is used to study the contributions that limit the time resolution regarding the crystal and the photodetector properties, to assess possible improvements and the potential of the materials. The measurement performed with the 3 × 3 × 20 mm^3

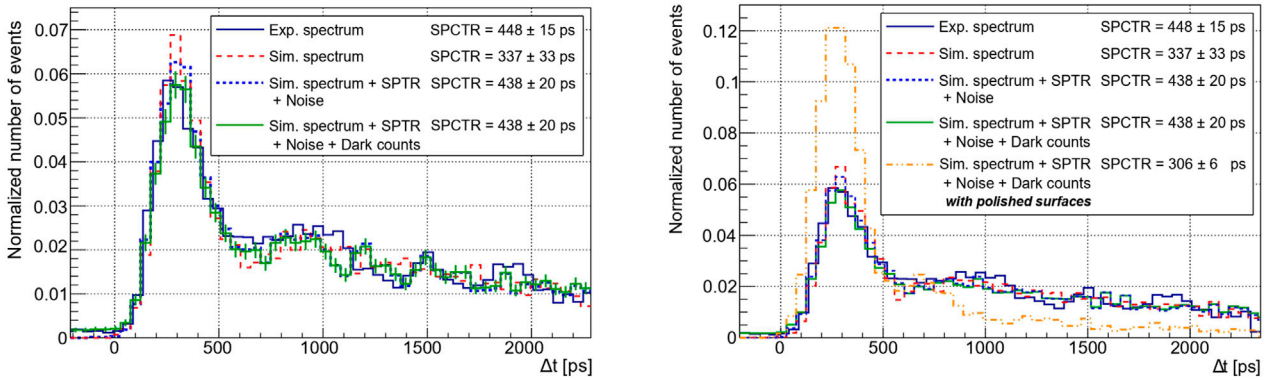

FIGURE 7 | (A) Simulation of the photodetector contributions affecting SPCTR and their impact on the coincidence time distribution, selecting events with one detected photon. The Teflon-wrapped TlBr crystal with dimensions 3 × 3 × 20 mm^3 is considered, with the 3 × 3 mm^2 side in coincidence with the reference detector. The corresponding measured time distribution is shown in superposition. **(B)** Comparison with the simulated time distribution assuming the crystal with polished surfaces.

Teflon-wrapped TlBr crystal is considered. Placing the 3 × 3 mm^2 face in coincidence with the reference detector, the CTR extracted after time-walk correction, assuming two equal detectors in coincidence, is 285 ± 9 ps (**Table 2**). If events with one-triggered SPAD only are selected, the resulting time distribution, shown on the left of **Figure 7** with the solid blue line, has a resolution (SPCTR) of 448 ± 15 ps.

This setup is simulated selecting events in which one photon only is detected and calculating the SPCTR according to **Eq. (1)**. Simulations are performed considering, initially, an ideal photodetector having no electronic noise and SPTR equal to 0 ps (red dashed line in **Figure 7**). The SPCTR, in this case, is 337 ± 33 ps FWHM. When adding SPTR and electronic noise, SPCTR becomes 438 ± 20 ps FWHM (blue dashed line). Finally, dark counts are added as a constant component to match the experimental spectrum (green line). In this case, SPCTR does not change, since the time resolution is always calculated as the FWHM of the distribution, subtracting for the baseline. The value 438 ± 20 ps is in agreement with the SPCTR extracted from the experimental measurement. Indeed, a good agreement is observed in **Figure 7**. The SiPM SPTR has a significant impact on the overall detector performance. The impact of the PDE is analyzed in the following section, when all events, regardless of the number of detected photons, are considered. Moreover, the simulation is repeated considering a polished crystal by setting both σ_α parameters to 0.005. The extracted SPCTR = 306 ± 6 ps proves that, currently, the major improvement can be achieved by polishing the surface of the crystal.

4 DISCUSSION

4.1 Impact of the Surface State on the Coincidence Time Resolution

The surface condition plays a fundamental role in time resolution [31, 32]. Unpolished surfaces have a greater tendency to promote internal reflection, as observed in the transmission plot in **Figure 1**, thus decreasing the number of photons lost (**section 4.2**) but severely increasing the PTS (**Figure 7**). **Table 2** shows that the CTR values measured with TlCl and TlBr are compatible, while a significant difference is found with the resolution of PbF_2. One of the sources of this difference is the surface state. Indeed, while TlBr and TlCl present unpolished surfaces, PbF_2 presents polished.

4.2 Impact of the Refractive Index on the Coincidence Time Resolution

The difference between the CTR values measured with TlCl/TlBr and PbF_2 is justified, on the one hand, by the difference in the surface state. On the other hand, this can be explained by the difference in the refractive index of the thallium-based crystals compared to PbF_2 (n = 2.32, 2.48 vs. n = 1.78), which promotes better extraction of photons in the latter, and by the different transmission cutoffs. TlBr and TlCl, unlike PbF_2, do not harvest Cherenkov photons between 300 and 400 nm. To study the contribution of the refractive index on the Cherenkov photon yield and the timing performance, the developed simulation tool kit is used to simulate a small crystal wrapped in Teflon, with dimensions 3 × 3 × 3 mm^3. Regarding the constituent material, all the properties of TlBr are considered except for the refractive index, which is modified performing a scan in the range 1.7–2.6, and the transmission cutoff set to 300 nm wavelength. Polished and unpolished surfaces are investigated, considering the two cases previously described. The coincidence with the reference detector is implemented. The CTR of the corresponding output time distribution and the number of detected photons are extracted. Despite the increasing number of produced Cherenkov photons as a function of the refractive index n [34] as

$$N_{produced} \sim 1 - \frac{1}{n^2}, \tag{6}$$

it is observed that the impact of the high refractive index on the CTR is almost negligible in the crystals with polished faces, while it shows a deterioration with the increasing refractive index for crystals with unpolished surfaces (**Figure 8**). At the same time, the mean number of detected photons is consistently greater in crystals with unpolished surfaces. These results suggest that, for crystals with unpolished surfaces, a greater fraction of photons undergoes more internal reflections before detection as the

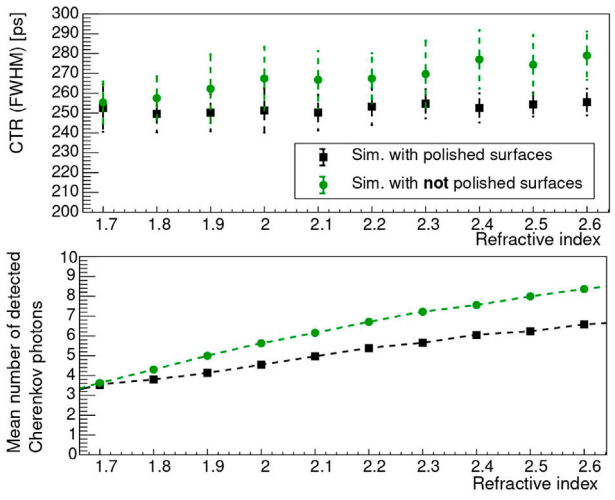

FIGURE 8 | Simulation results on the mean number of detected Cherenkov photons and CTR as a function of the refractive index.

refractive index increases, while in crystals with polished surfaces these additional events are not detected.

4.3 Impact of the SiPM on the Coincidence Time Resolution

From the photodetector side, relevant contributions to the CTR arise from the time response of the detection (SPTR), electronic noise, and PDE. To evaluate their impact on time resolution, simulations are performed using two different crystal geometries ($3 \times 3 \times 3$ mm^3 and $3 \times 3 \times 20$ mm^3). The crystal properties are fixed to those of Teflon-wrapped TlBr and the σ_α parameters to 0.005, while the SPTR and PDE of the SiPM are varied. To simplify the analysis, the time delay distribution is considered in coincidence with a perfect reference detector (CTR = 0 ps), and the standard deviation within a fixed time window is saved as the figure of merit for the time resolution. The time delay distributions simulated for three specific (PDE [%], SPTR (FWHM) [ps]) values, with a short crystal and a long crystal, are displayed at the top of **Figure 9**. In particular, the case of a perfect PDE (100%) and a very good SPTR (50 ps FWHM) is compared to the case of a SiPM having a worse SPTR (100 ps FWHM) or a worse PDE (1%). While a high SPTR introduces only a spread in the time distribution, clearly visible on the peak, a low PDE increases the fraction of events in the tail, due to the low probability of detecting the fastest optical photon.

Varying the PDE in steps of 1% and the SPTR in steps of 2 ps FWHM, the resulting heat maps are shown at the bottom of **Figure 9**, where the isolines represent a change of 10 ps in standard deviation. The three black dots represent typical values of the parameters of different photodetectors, namely SiPMs from FBK (NUV-HD) and Hamamatsu (HPK S13360–3050 PE) [2] and an MCP-PMT with excellent time response but worse detection efficiency [14]. It is observed that, for the small crystal geometry, SPTR dominates the overall time performance, while PDE is less important. This is also the reason for the excellent measured CTR values in [14] for using small black-painted crystals. However, when approaching

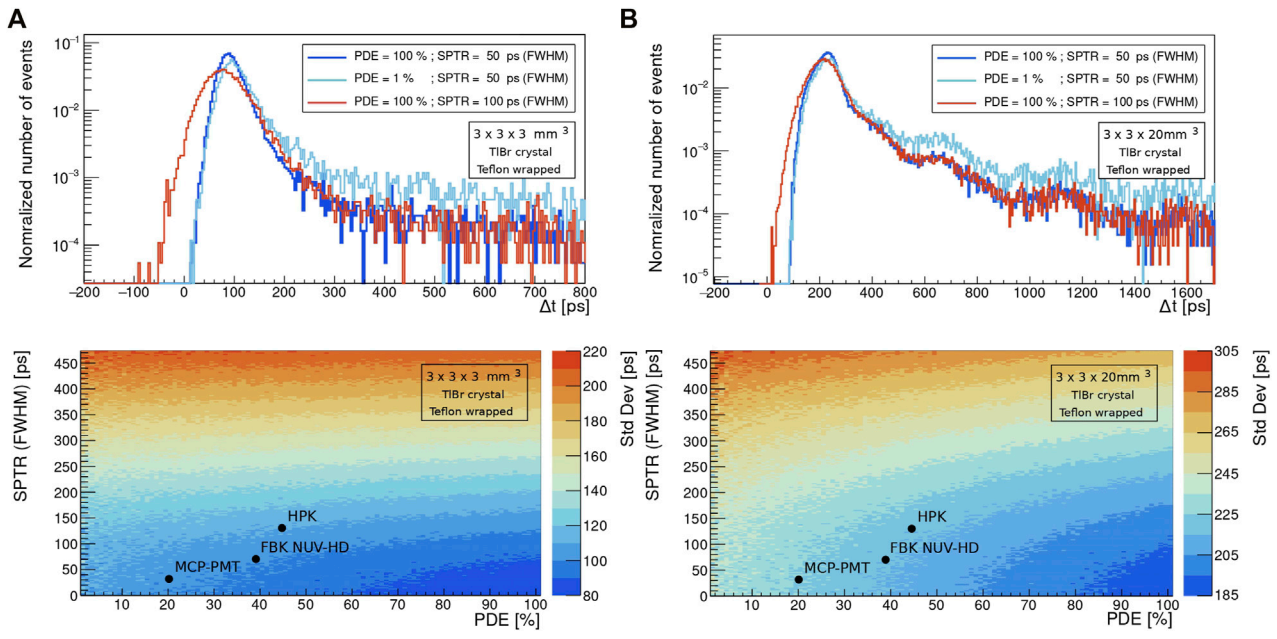

FIGURE 9 | (Top) Simulated time delay distributions considering three specific [PDE (%), SPTR (FWHM) (ps)] pairs: (100, 50), (1, 50), and (100, 100), for **(A)** a 3 mm and **(B)** 20 mm long crystal. (Bottom) Standard deviation of the simulated output time distributions as a function of the PDE and SPTR for the two different crystal lengths, **(A)** 3 mm and **(B)** 20 mm.

PET-sized geometry with longer crystals, it becomes clear that more attention needs to be drawn on the detection efficiency, possibly making SiPMs a more favorable choice of photodetector compared to fast MCP-PMTs.

4.4 Limitations of This Study and Future Work

Assuming two equal detectors in coincidence, CTR values of about 210 ps FWHM are measured with small Teflon-wrapped TlBr and TlCl crystals. These values are significantly better compared to those around 400 ps reported in the literature [11, 13], despite the acceptance of all events, without any selection on the number of triggered SPADs. The coincidence time resolution setup used differs from that described in the literature in using a SiPM with a better SPTR, higher SiPM overvoltage, and high bandwidth readout. In particular, FBK NUV-HD with an intrinsic SPTR $\approx$ 70 ps is used compared to HPK S14160 with an intrinsic SPTR $\approx$ 120 ps [2]. Good SPTR and high bandwidth readout are crucial to optimize the timing performance in the case of low light intensities [20, 25]. In addition, time-walk correction significantly improves the timing performance. This correction method could have a practical implementation in an ASIC with two trigger levels, where the first is used as the primary time-stamp and the second to calculate the slew rate around the leading edge threshold [35]. However, the measured CTR values can be further optimized, by polishing the crystal and improving light transfer and light collection.

In the simulations, a digital-like approach is used for the SiPM, and the impact of optical cross talk is ignored, focusing on one-triggered SPAD events. Both simplifications provide valid results. However, the study of the analog SiPM response and the model of SiPM cross talk in the case of a few detected photons would provide more accurate results and will be subjected to future work.

5 CONCLUSION

This work advanced the understanding of high refractive index Cherenkov radiators and light propagation in these crystals through experimental measurements and simulations. Despite the relatively low transparency of semiconductor materials in the UV region, where most of the Cherenkov photons are produced, time resolutions significantly below 200 ps FWHM are measured. This is in line with simulation results and defines a new state of the art for such materials. Following this, a double-sided readout will be investigated to mitigate the contribution of back-reflected photons and to maximize detection efficiency. In addition, the use of the charge induction readout could enable accurate energy discrimination to effectively select events with higher energy depositions, which show a greater generation yield of Cherenkov photons. This would further improve the time resolution, making CTR values close to 100 ps achievable for a substantial fraction of events.

DATA AVAILABILITY STATEMENT

The raw data supporting the conclusion of this article will be made available by the authors, without undue reservation.

AUTHOR CONTRIBUTIONS

GT, GA-E, ER, and NK developed, as a team, the idea of studying the timing capabilities of Cherenkov semiconductors. The simulation framework was developed by GT, MP, and NK, and the experimental measurements were carried out by GT and NK. The crystals used for the measurements were provided by ER, SC, JG, KS, and GA-E. GT performed data analysis and wrote the manuscript. The supervision, resources, and accurate review of the manuscript were provided by SC, EA, AG, NK, MP, ER, JG, KS, and GA-E.

ACKNOWLEDGMENTS

This work has been performed in the framework of the Crystal Clear Collaboration. The authors thank FBK (Alberto Gola and Maria Ruzzarin) for the SiPM samples used for this work. Furthermore, we want to express our gratitude to Stefan Gundacker for the preparation of the CTR experimental setup and high-frequency electronics.

REFERENCES

1. Schaart DR. Physics and Technology of Time-Of-Flight PET Detectors. *Phys Med Biol* (2021) 66:09TR01. doi:10.1088/1361-6560/abee56
2. Gundacker S, Martinez Turtos R, Kratochwil N, Pots RH, Paganoni M, Lecoq P, et al..Experimental Time Resolution Limits of Modern SiPMs and TOF-PET Detectors Exploring Different Scintillators and Cherenkov Emission. *Phys Med Biol* (2020) 65:025001. doi:10.1088/1361-6560/ab63b4
3. Gundacker S, Pots RH, Nepomnyashchikh A, Radzhabov E, Shendrik R, Omelkov S, et al..Vacuum Ultraviolet Silicon Photomultipliers Applied to BaF2 Cross-Luminescence Detection for High-Rate Ultrafast Timing Applications. *Phys Med Biol* (2021) 66:114002. doi:10.1088/1361-6560/abf476
4. Kratochwil N, Gundacker S, Lecoq P, Auffray E. Pushing Cherenkov PET with BGO via Coincidence Time Resolution Classification and Correction. *Phys Med Biol* (2020) 65:115004. doi:10.1088/1361-6560/ab87f9
5. Pizzichemi M, Polesel A, Stringhini G, Gundacker S, Lecoq P, Tavernier S, et al..On Light Sharing TOF-PET Modules with Depth of Interaction and 157 Ps FWHM Coincidence Time Resolution. *Phys Med Biol* (2019) 64:155008. doi:10.1088/1361-6560/ab2cb0
6. Du J, Ariño-Estrada G, Bai X, Cherry SR. Performance Comparison of Dual-Ended Readout Depth-Encoding PET Detectors Based on BGO and LYSO Crystals. *Phys Med Biol* (2020) 65:235030. doi:10.1088/1361-6560/abc365
7. Kim H, Cirignano L, Churilov A, Ciampi G, Higgins W, Olschner F, et al..Developing Larger TlBr Detectors-Detector Performance. *IEEE Trans Nucl Sci* (2009) 56:819–23. doi:10.1109/TNS.2009.2014756

8. Kim H, Ogorodnik Y, Kargar A, Cirignano L, Thrall CL, Koehler W, et al..Thallium Bromide Gamma-ray Spectrometers and Pixel Arrays. *Front Phys* (2020) 8:55. doi:10.3389/fphy.2020.00055
9. Ariño-Estrada G, Mitchell GS, Kwon SI, Du J, Kim H, Cirignano LJ, et al..Towards Time-Of-Flight PET with a Semiconductor Detector. *Phys Med Biol* (2018) 63:04LT01. doi:10.1088/1361-6560/aaaa4e
10. Gundacker S, Auffray E, Pauwels K, Lecoq P. Measurement of Intrinsic Rise Times for Various L(Y)SO and LuAG Scintillators with a General Study of Prompt Photons to Achieve 10 Ps in TOF-PET. *Phys Med Biol* (2016) 61: 2802–37. doi:10.1088/0031-9155/61/7/2802
11. Ariño-Estrada G, Mitchell GS, Kim H, Du J, Kwon SI, Cirignano LJ, et al..First Cerenkov Charge-Induction (CCI) TlBr Detector for TOF-PET and Proton Range Verification. *Phys Med Biol* (2019) 64:175001. doi:10.1088/1361-6560/ab35c4
12. Ariño-Estrada G, Kim H, Du J, Cirignano LJ, Shah KS, Cherry SR. Energy and Electron Drift Time Measurements in a Pixel CCI TlBr Detector with 1.3 MeV Prompt-Gammas. *Phys Med Biol* (2021) 66:044001. doi:10.1088/1361-6560/abd419
13. Ariño-Estrada G, Roncali E, Selfridge AR, Du J, Glodo J, Shah KS, et al..Study of Čerenkov Light Emission in the Semiconductors TlBr and TlCl for TOF-PET. *IEEE Trans Radiat Plasma Med Sci* (2021) 5:630–7. doi:10.1109/TRPMS.2020.3024032
14. Ota R, Nakajima K, Ogawa I, Tamagawa Y, Shimoi H, Suyama M, et al..Coincidence Time Resolution of 30 Ps FWHM Using a Pair of Cherenkov-Radiator-Integrated MCP-PMTs. *Phys Med Biol* (2019) 64: 07LT01. doi:10.1088/1361-6560/ab0fce
15. Dolenec R, Korpar S, Križan P, Pestotnik R. Cherenkov TOF PET with Silicon Photomultipliers. *Nucl Instr Methods Phys Res Section A: Acc Spectrometers, Detectors Associated Equipment* (2015) 804:127–31. doi:10.1016/j.nima.2015.09.059
16. Kratochwil N, Gundacker S, Auffray E. A Roadmap for Sole Cherenkov Radiators with SiPMs in TOF-PET. *Phys Med Biol* (2021) 66:195001. doi:10.1088/1361-6560/ac212a
17. Gola A, Acerbi F, Capasso M, Marcante M, Mazzi A, Paternoster G, et al..NUV-sensitive Silicon Photomultiplier Technologies Developed at Fondazione Bruno Kessler. *Sensors* (2019) 19:308. doi:10.3390/s19020308
18. Gundacker S, Turtos RM, Auffray E, Paganoni M, Lecoq P. High-frequency SiPM Readout Advances Measured Coincidence Time Resolution Limits in TOF-PET. *Phys Med Biol* (2019) 64:055012. doi:10.1088/1361-6560/aafd52
19. Murty RC. Effective Atomic Numbers of Heterogeneous Materials. *Nature* (1965) 207:398–9. doi:10.1038/207398a0
20. Cates JW, Gundacker S, Auffray E, Lecoq P, Levin CS. Improved Single Photon Time Resolution for Analog SiPMs with Front End Readout that Reduces Influence of Electronic Noise. *Phys Med Biol* (2018) 63:185022. doi:10.1088/1361-6560/aadbcd
21. Dolenec R, Korpar S, Križan P, Pestotnik R. SiPM Timing at Low Light Intensities. In: 2016 IEEE Nuclear Science Symposium, Medical Imaging Conference and Room-Temperature Semiconductor Detector Workshop (NSS/MIC/RTSD), Strasbourg, France, October 29–November 6, 2016 (2016). p. 1–5. doi:10.1109/NSSMIC.2016.8069832
22. Stockhoff M, Jan S, Dubois A, Cherry SR, Roncali E. Advanced Optical Simulation of Scintillation Detectors in GATE v8.0: First Implementation of a Reflectance Model Based on Measured Data. *Phys Med Biol* (2017) 62: L1–L8. doi:10.1088/1361-6560/aa7007
23. Roncali E, Stockhoff M, Cherry SR. An Integrated Model of Scintillator-Reflector Properties for Advanced Simulations of Optical Transport. *Phys Med Biol* (2017) 62:4811–30. doi:10.1088/1361-6560/aa6ca5
24. Schaart DR, Ziegler S, Zaidi H. Achieving 10 Ps Coincidence Time Resolution in TOF-PET Is an Impossible Dream. *Med Phys* (2020) 47:2721–4. doi:10.1002/mp.14122
25. Kratochwil N, Auffray E, Gundacker S. Exploring Cherenkov Emission of BGO for TOF-PET. *IEEE Trans Radiat Plasma Med Sci* (2021) 5:619–29. doi:10.1109/TRPMS.2020.3030483
26. Toussaint M, Loignon-Houle F, Dussault J-P, Lecomte R. Analytical Model of DOI-Induced Time Bias in Ultra-fast Scintillation Detectors for TOF-PET. *Phys Med Biol* (2019) 64:065009. doi:10.1088/1361-6560/ab038b
27. Cates JW, Vinke R, Levin CS. Analytical Calculation of the Lower Bound on Timing Resolution for PET Scintillation Detectors Comprising High-Aspect-Ratio crystal Elements. *Phys Med Biol* (2015) 60:5141–61. doi:10.1088/0031-9155/60/13/5141
28. Gundacker S, Acerbi F, Auffray E, Ferri A, Gola A, Nemallapudi MV, et al..State of the Art Timing in TOF-PET Detectors with LuAG, GAGG and L(y)SO Scintillators of Various Sizes Coupled to FBK-SiPMs. *J Inst* (2016) 11:P08008. doi:10.1088/1748-0221/11/08/p08008
29. Loignon-Houle F, Gundacker S, Toussaint M, Camirand Lemyre F, Auffray E, Fontaine R, et al..DOI Estimation through Signal Arrival Time Distribution: a Theoretical Description Including Proof of Concept Measurements. *Phys Med Biol* (2021) 66:095015. doi:10.1088/1361-6560/abf604
30. Gundacker S, Knapitsch A, Auffray E, Jarron P, Meyer T, Lecoq P. Time Resolution Deterioration with Increasing crystal Length in a Tof-Pet System. *Nucl Instr Methods Phys Res Section A: Acc Spectrometers, Detectors Associated Equipment* (2014) 737:92–100. doi:10.1016/j.nima.2013.11.025
31. Berg E, Roncali E, Cherry SR. Optimizing Light Transport in Scintillation Crystals for Time-Of-Flight Pet: an Experimental and Optical Monte Carlo Simulation Study. *Biomed Opt Express* (2015) 6:2220–30. doi:10.1364/BOE.6.002220
32. Kang HG, Yamaya T, Han YB, Song SH, Ko GB, Lee JS, et al..Crystal Surface and Reflector Optimization for the SiPM-Based Dual-Ended Readout TOF-DOI PET Detector. *Biomed Phys Eng Express* (2020) 6:065028. doi:10.1088/2057-1976/abc45a
33. Gonzalez-Montoro A, Pourashraf S, Lee MS, Cates JW, Levin CS. Study of Optical Reflectors for a 100ps Coincidence Time Resolution TOF-PET Detector Design. *Biomed Phys Eng Express* (2021) 7:065008. doi:10.1088/2057-1976/ac240e
34. Brunner SE, Schaart DR. BGO as a Hybrid Scintillator/Cherenkov Radiator for Cost-Effective Time-Of-Flight PET. *Phys Med Biol* (2017) 62:4421–39. doi:10.1088/1361-6560/aa6a49
35. Gomez S, Fernandez-Tenllado JM, Alozy J, Campbell M, Manera R, Mauricio J, et al..FastIC: A Highly Configurable ASIC for Fast Timing Applications. In: IEEE NSS/MIC conference record 2021, Yokohama, Japan, October 16–23. 2021 (2021).

Conflict of Interest: Authors JG and KS were employed by Radiation Monitoring Devices, Inc.

The remaining authors declare that the research was conducted in the absence of any commercial or financial relationships that could be construed as a potential conflict of interest.

Publisher's Note: All claims expressed in this article are solely those of the authors and do not necessarily represent those of their affiliated organizations, or those of the publisher, the editors, and the reviewers. Any product that may be evaluated in this article, or claim that may be made by its manufacturer, is not guaranteed or endorsed by the publisher.